# Yeast silencing factor Sir4 and a subset of nucleoporins form a complex distinct from nuclear pore complexes

Diego L. Lapetina, Christopher Ptak, Ulyss K. Roesner, and Richard W. Wozniak

Department of Cell Biology, University of Alberta, Edmonton, Alberta, Canada

Interactions occurring at the nuclear envelope (NE)–chromatin interface influence both NE structure and chromatin organization. Insights into the functions of NE–chromatin interactions have come from the study of yeast subtelomeric chromatin and its association with the NE, including the identification of various proteins necessary for tethering subtelomeric chromatin to the NE and the silencing of resident genes. Here we show that four of these proteins—the silencing factor Sir4, NE-associated Esc1, the SUMO E3 ligase Siz2, and the nuclear pore complex (NPC) protein Nup170—physically and functionally interact with one another and a subset of NPC components (nucleoporins or Nups). Importantly, this group of Nups is largely restricted to members of the inner and outer NPC rings, but it lacks numerous others including cytoplasmically and nucleoplasmically positioned Nups. We propose that this Sir4-associated Nup complex is distinct from holo-NPCs and that it plays a role in subtelomeric chromatin organization and NE tethering.

## Introduction

In eukaryotic cells, chromatin is sequestered from the cytoplasm by the nuclear envelope (NE), a double-membrane structure composed of an outer nuclear membrane (ONM) exposed to the cytoplasm and an inner nuclear membrane (INM) exposed to the nucleoplasm. Each bilayer houses a unique set of proteins that define ONM- and INM-localized functions (Stancheva and Schirmer, 2014). Nuclear pore complexes (NPCs), numbering ~100 in a haploid yeast NE (Winey et al., 1997), interrupt the NE surface and extend across the NE through pores formed by the fusion of the INM and ONM. The cylindrically shaped NPCs are ~100 nm in diameter and are composed of multiple copies of ~30 different proteins termed nucleoporins or Nups (Aitchison and Rout, 2012). The major structural feature of the NPC is the cylindrical core scaffold. Composed of the most highly conserved Nups, the core scaffold is made up of eight spoke structures of identical composition that lie adjacent to the pore membrane and form a flexible framework for the central channel of the NPC. Built on the core are numerous other Nups, including those that bind to the nuclear transport factors and that line the channel or are positioned specifically on the cytoplasmic face of the NPC or the nucleoplasmic face adjacent to chromatin.

In addition to their functions in nuclear transport, Nups with access to the nucleoplasm, together with proteins that populate the INM, are positioned to interact with and sequester chromatin along the two-dimensional surface of the INM (Ptak

et al., 2014; Czapiewski et al., 2016; Gonzalez-Sandoval and Gasser, 2016; Ptak and Wozniak, 2016). In yeast and metazoan cells, transcriptionally silent heterochromatin is a prominent interacting partner of INM proteins and a few Nups, whereas transcriptionally active chromatin concentrates at NPCs and binds a subset of Nups. Yeast has provided an important model for the study of chromatin interactions with the NE, and among the most well studied of these interactions is the binding of telomeres and subtelomeric chromatin with the NE. In addition to its role in genome organization, telomere tethering is functionally linked to subtelomeric gene silencing, telomere length regulation, and the repair of persistent DNA damage at telomeres (Taddei and Gasser, 2012; Kupiec, 2014; Marcomini and Gasser, 2015; Ptak and Wozniak, 2016). NE-tethering interactions use multiple protein/DNA complexes along telomeric and subtelomeric regions. Among the chromatin-associated factors that contribute to these binding events are the telomerase complex and the yKu complex, which bind chromosome ends; Rap1, which coats the TG repeat region of telomeres and recruits the silent information regulator (SIR) complex; and the SIR complex itself, which binds distinct regions within subtelomeric chromatin (Taddei and Gasser, 2012; Kupiec, 2014). These telomeric and subtelomeric complexes associate with distinct NE-associated proteins including Esc1, which interacts with the SIR complex through Sir4, and the integral membrane protein Mps3, which has been proposed to bind Sir4 and the yKu/

telomerase complex (Andrulis et al., 2002; Taddei et al., 2004). These multiple tethering mechanisms appear to function preferentially at distinct periods of the cell cycle (Andrulis et al., 2002; Taddei et al., 2004; Bupp et al., 2007). However, the functional relevance of these multiple pathways remains to be determined.

Yeast Nups have also been linked to the regulation of telomere tethering, subtelomeric silencing, telomere length, and DNA repair at telomeres. In one study, mutations in members of the Nup84 subcomplex were shown to exhibit defects in telomere tethering, gene silencing, and DNA repair (Therizols et al., 2006). Recent work has also established a direct physical link between subtelomeric chromatin and Nup170, a component of the inner rings of the NPC core scaffold (Van de Vosse et al., 2013). Nup170 interacts with Sir4 and functions in the tethering of both Sir4 and telomeres to the NE. Moreover, mutant cells lacking Nup170 exhibit defects in subtelomeric gene silencing and the binding of Sir4 to subtelomeric chromatin, suggesting that Nup170 functions in the assembly of Sir4 onto subtelomeric chromatin. These observations have led to the conclusion that NPCs functionally interact with subtelomeric regions of the yeast genome.

The tethering of yeast telomeres to the NE appears to be a highly dynamic process, as telomeres move both within the two-dimensional plane of the NE and on and off the NE (Rosa et al., 2006; Conrad et al., 2008; Ebrahimi and Donaldson, 2008). In the latter case, individual telomeres are detected leaving the NE and moving into the nucleoplasm for variable lengths of time during interphase. Moreover, they are released from the NE in late S phase when telomeres replicate (Gilson and Géli, 2007). This dynamic behavior may be driven by posttranslational modifications. In this regard, SUMOylation has emerged as a regulator of telomere function in that the SUMO E3 ligase Siz2 is required for telomere tethering to the NE and telomere length regulation (Ferreira et al., 2011). Several proteins involved in telomere regulation are SUMOylated (Wohlschlegel et al., 2004; Denison et al., 2005), including Sir4, yKu80, and Sir2, each of which is predominantly targeted for SUMOylation by Siz2 (Ferreira et al., 2011; Hannan et al., 2015). SUMOylation has also been suggested to regulate the distribution of Sir2 between telomeres and ribosomal DNA in the nucleolus, and in this way Siz2 might control the degree of heterochromatin assembly within these regions (Hannan et al., 2015).

The multiple factors that contribute to the tethering of telomeres and subtelomeric chromatin to the NE highlight the complex nature of these interactions. Although certain functions have been ascribed to individual anchoring factors, the physical and temporal interactions between these various NE proteins, as well as their ability to function independently or together within tethering complexes, have not been explored. Understanding these relationships remains an important unresolved issue as we look to understand the functional significance of chromatin tethering to the NE. This challenging problem is further complicated by the observation that NE tethering proteins, such as Mps3, Esc1, and Nup170, populate regions of the NE that both overlap with and are distinct from Sir4 and telomere clusters (Andrulis et al., 2002; Taddei et al., 2004; Bupp et al., 2007; Van de Vosse et al., 2013), suggesting that these proteins exist in multiple complexes. In this study, we have investigated the physical interactions of chromatin-associated Sir4 with various NE proteins. We identified a protein interaction network containing Sir4, Esc1, Siz2, Nup170, and several additional Nups.

This group of Nups contains members of the membrane-bound core scaffold but lacks Nups from other NPC subcomplexes. Importantly, we show that these Sir4-associated Nup (Snup) complexes are separate entities positioned along the NE and distinct from holo-NPCs.

## Results

### Nup170 interacts with proteins functioning in telomere localization to the NE

The nucleoporin Nup170 binds subtelomeric chromatin (regions within 20 kb of chromosome ends) and is required for normal subtelomeric gene silencing and telomere tethering to the NE (Van de Vosse et al., 2013). Closer inspection of Nup170 binding sites within subtelomeric chromatin reveals that this Nup is enriched at distinct sites within these regions. Strikingly, a comparison of the Nup170 chromatin binding profile with a recently published chromatin immunoprecipitation sequencing (ChIP-seq) dataset for SIR complex components (Ellahi et al., 2015) reveals that the majority of these binding sites overlap (Fig. 1). These data are consistent with the previously reported physical association between Sir4 and Nup170 and the observed role of Sir4 in mediating Nup170 binding to subtelomeric chromatin (Van de Vosse et al., 2013).

Apart from Nup170, Sir4 also interacts with other proteins at the NE, including two membrane-associated proteins, Esc1 and Mps3, implicated in anchoring telomeres to the NE (Andrulis et al., 2002; Bupp et al., 2007). Whether these proteins are present in one or multiple Sir4-containing complexes is unclear. To address this, we investigated the physical interactions between Nup170, Esc1, Mps3, and Sir4. To do this, the endogenous gene encoding Sir4, Esc1, or Mps3 was modified to produce a C-terminally tagged protein A (PrA) fusion. The PrA-fusion proteins were affinity purified from cell extracts and probed for copurifying proteins that interact directly or indirectly with the PrA fusions. Consistent with previous studies suggesting that Esc1 and Mps3 interact with Sir4, we detected Sir4 bound to Esc1-PrA and Mps3-PrA (Fig. 2, A and B). However, Nup170 was detected only in association with Esc1-PrA, but not Mps3-PrA. Purification of Sir4-PrA also revealed associated Nup170 and Esc1 (Fig. 2 C). These data and previous observations (Van de Vosse et al., 2013) are consistent with the existence of a complex containing Sir4, Esc1, and Nup170.

To further assess the physical association between Nup170, Esc1, and Sir4, we examined the effect of losing one of these three proteins on the association of the two remaining proteins. To test this, Esc1-PrA or Sir4-PrA was affinity purified from cellular extracts of a strain containing a *sir4Δ*, *nup170Δ*, or *esc1Δ* null mutation (Fig. 3). Collectively, comparison of coaffinity purifications from WT cell extracts with those from mutant cell extracts revealed that the absence of any one member of this trio of proteins led to specific and reproducible changes in the association of the two remaining proteins. We observed that the amount of Nup170 associated with Esc1-PrA was reduced in strains lacking Sir4 (Figs. 3 A and S1 A) but was unaltered by the loss of the Nup170 binding partner Nup53 (not depicted). In contrast, purified Esc1-PrA showed increased amounts of associated Sir4 in the absence of Nup170 (Figs. 3 B and S1 A). We also examined the effect of the *esc1Δ* mutant on the association of Sir4-PrA with Nup170. In this case, we observed a reproducible decrease in the levels of Nup170
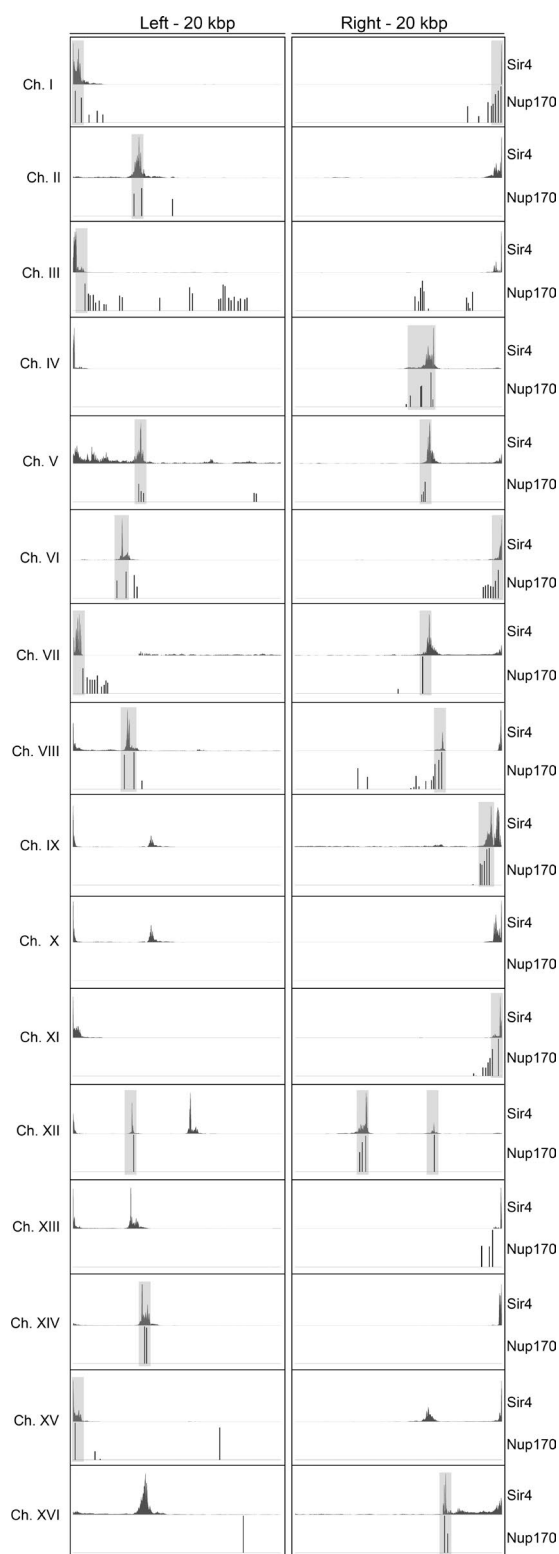
Figure 1. **Sir4 and Nup170 enrich at similar regions within subtelomeric chromatin.** Previously reported Sir4 ChIP-Seq (Ellahi et al., 2015; top track) and Nup170 ChIP-chip (Van de Vosse et al., 2013; bottom track) data are compared within the first (left) and last (right) 20 kbp of each of the 16 yeast chromosomes (i.e., 32 telomeres). Peak heights correspond to fold enrichment as defined in these studies. Data are represented in sacCer1 genome with a resolution of 5 bp (Sir4) and 56 bp (Nup170). Note that six telomeric regions (IX-L, X-L, X-R, XV-R, XIV-L, and XVI-L) had too few probes to accurately represent Nup170 enrichment. Sir4 and Nup170 enrichment in similar regions is highlighted in light gray.
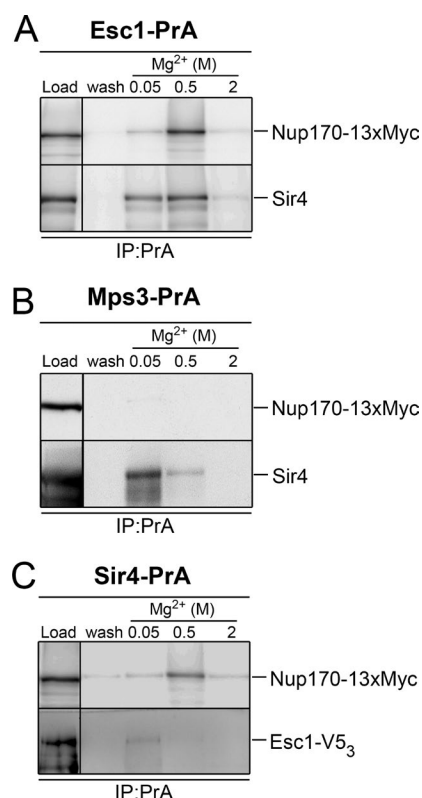


Figure 2. **Nup170 is associated with Esc1 and Sir4, but not Mps3.** Extracts from cells producing Nup170-13xMyc and Esc1-PrA (A) or Mps3-PrA (B), as well as extracts from cells producing Sir4-PrA, Nup170-13xMyc, and Esc1-V5$_3$ (C), were used as starting material for purification of the indicated PrA fusions. Extracts (load) were mixed with IgG beads to bind the PrA fusion. After the final wash, proteins were eluted with buffer containing increasing MgCl$_2$ (Mg$^{2+}$) concentrations of 0.05, 0.5, and 2 M. Samples from each step were analyzed by Western blotting using antibodies directed against the Myc and V5 peptides and Sir4.

recovered in association with Sir4-PrA (Figs. 3 C and S1 A). Of note, changes in the affinity purification profiles in the mutants were observed as alterations in the amount of the interacting partner bound to the PrA-fusion rather than a change in the relative proportion of purified protein that eluted at each Mg$^{2+}$ concentration (Fig. 3, A–C). These results are consistent with the idea that the loss of one member of this group of proteins is less likely to affect the strength of the interactions between the remaining two proteins, but rather influences the accessibility of these proteins to one another. Together, these experiments show that Nup170, Esc1, and Sir4 exhibit multiple interactions that are interdependent.

## The subcellular localizations of Sir4, Esc1, and Nup170 are interdependent

Copurification results led us to conclude that Nup170, Esc1, and Sir4 are members of a protein complex. To expand on this idea, we examined the interdependence of these proteins on their subcellular distribution. To test this, the endogenous gene coding for each protein was modified to produce Esc1-eGFP, Sir4-eGFP, or Nup170-eGFP in WT cells and mutant cells lacking one of the other interacting partners (*nup170Δ*, *sir4Δ*, or *esc1Δ*). In WT cells, Esc1-eGFP exhibited a punctate distribution along the NE, but was excluded from regions adjacent to the nucleolus (detected with the nucleolar marker Nop1-RFP;
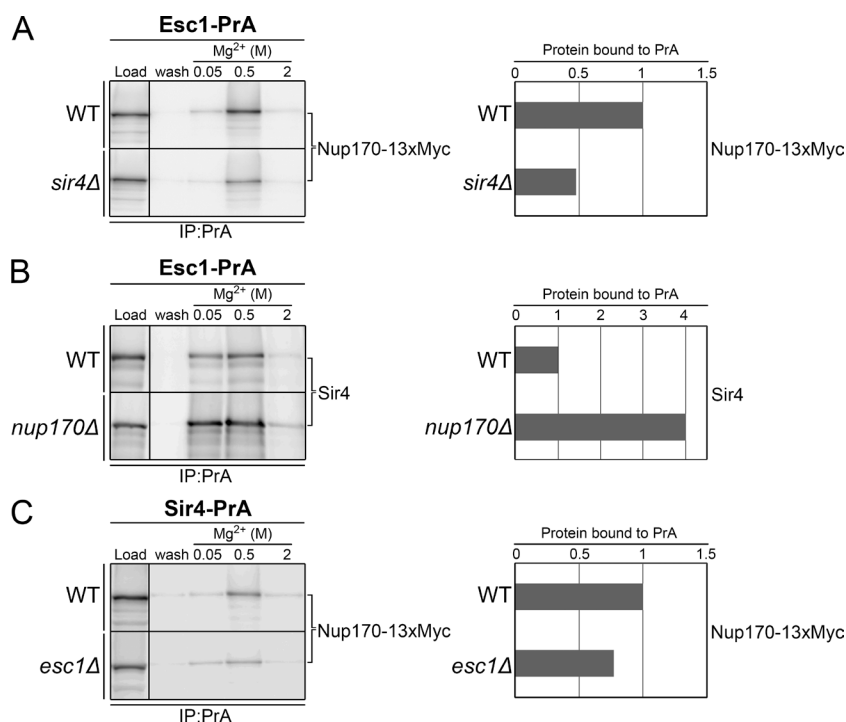
Figure 3. **Interactions between Nup170, Esc1, and Sir4 are altered in deletion mutants.** PrA fusions were affinity purified from cell extracts derived from WT and deletion mutant strains producing Esc1-PrA and Nup170-13xMyc (WT and *sir4Δ*; A), Esc1-PrA (WT and *nup170Δ*; B), or Sir4-PrA and Nup170-13xMyc (WT and *esc1Δ*; C). Analysis of the indicated fractions by Western blotting (left) was performed as described in Fig. 2. Signals derived from these Western blots were quantified (see Materials and methods), and results are shown in the adjacent bar graphs. The ratio of the bound protein to PrA fusion in the WT strain was assigned a value of 1. Decreased or increased ratios of copurifying protein relative to the bound PrA fusion are indicated. Note that (a) the cellular levels of Nup170-13xMyc and Sir4 (see load fractions) and the PrA fusions were similar in the WT and mutant cells (not depicted); and (b) biological replicates of the affinity purification experiments shown here are presented in Fig. S1.

Fig. 4 A), similar to previous studies (Andrulis et al., 2002). This exclusion was clearly visible in ~70% of WT cells. However, exclusion dropped to ~40% of *sir4Δ* cells and ~30% of *nup170Δ* cells, with the latter also appearing to exhibit altered nucleolar structure (Fig. 4 A). These results suggest that both Sir4 and Nup170 contribute to the exclusion of Esc1 from regions of the NE that interact with the nucleolus.

Exclusion of Esc1-eGFP from the nucleolar-associated NE regions is also dependent on the NPC nuclear basket–associated proteins Mlp1 and Mlp2 (Lewis et al., 2007; Niepel et al., 2013). Therefore, we tested whether the loss of Nup170 indirectly affected the distribution of Esc1-eGFP by altering Mlp localization. This was not the case, as localization of the Mlps was not affected by the loss of Nup170 (Fig. S2), suggesting that Nup170 affects Esc1-eGFP localization without disrupting the integrity of the NPC nuclear basket.

Sir4-eGFP is bound to subtelomeric chromatin, and it is generally detected in 6–10 foci at the NE (Gotta et al., 1996; Luo et al., 2002). We examined the localization of Sir4-eGFP in growing cultures of WT, *esc1Δ*, and *nup170Δ* cells. In contrast to WT cells, *esc1Δ* and *nup170Δ* mutants showed a decrease in the number of Sir4-eGFP foci associated with the NE. The *esc1Δ* mutant showed defects in G1-phase cells (Fig. 4 B, WT vs. *esc1Δ*), whereas *nup170Δ* cells, in G1-phase and S-phase (Fig. 4 B), exhibited defects consistent with previous observations (Van de Vosse et al., 2013).

Finally, we also examined the consequences of *esc1Δ* and *sir4Δ* mutations on the localization of Nup170-eGFP. In *sir4Δ* cells, the localization of Nup170-eGFP and other representative Nup-eGFP fusions appeared similar to that of WT cells (Fig. 4 C), with each concentrated at the NE in a characteristic punctate distribution. In contrast, clusters of Nup170-eGFP signal, visible as bright foci along the NE, were seen in *esc1Δ* cells. A similar phenotype was also observed for Nup84-eGFP, which (as shown in Fig. 7) is also associated with a Nup170, Esc1, and Sir4 complex. However, this clustering pattern was not detected with Nup53-eGFP, an NPC binding partner of Nup170, and Pom34-eGFP (Fig. 4 C). Cumulatively, the analysis of the subcellular localization of Nup170-eGFP, together with those of Esc1-eGFP and Sir4-eGFP, further support the conclusion that Nup170, Esc1, and Sir4 physically interact at the nuclear periphery.

## The SUMO E3 ligase Siz2 interacts with Nup170 and Sir4

The physical interactions we detected between Nup170, Esc1, and Sir4 are consistent with each protein's involvement in the maintenance of subtelomeric chromatin structure and NE tethering. Recent studies have also reported that a SUMO ligase, Siz2, is required for Sir4 SUMOylation and the association of subtelomeric chromatin with the NE (Ferreira et al., 2011). Thus, we examined whether Siz2 is physically associated with Nup170, Esc1, and Sir4. Analysis of Siz2-PrA purified from cell extracts revealed association with Sir4 and Nup170, but not the Nup170-interacting partner Nup53 (Fig. 5 A). Consistent with these results, GFP-Siz2, although visible throughout the nucleoplasm as previously reported (Huh et al., 2003), was also detected at the NE where it overlapped with the NE marker Sur4-mCherry (Fig. 5 B).

Siz2 was also detected in association with purified Esc1-PrA (Fig. 5 C). Moreover, like Sir4 and Nup170, Siz2 was required for proper NE localization of Esc1. In a strain lacking Siz2, Esc1 was not efficiently excluded from regions of the NE adjacent to the nucleolus (Fig. 5 D). These results implied that the loss of Siz2 may alter the association of Nup170, Sir4, and Esc1 with one another. We tested this by examining the interactions of these proteins in strains lacking Siz2. Comparison of WT to *siz2Δ* cells revealed a reproducible reduction in the amount of Nup170 associated with Esc1-PrA in *siz2Δ* cells but little or no change in the amount of Nup170 coenriching with Sir4-PrA or of Sir4 with Esc1-PrA (Figs. 5 E and S1 B). Furthermore, the loss of Siz2 did not appear to influence the sub-
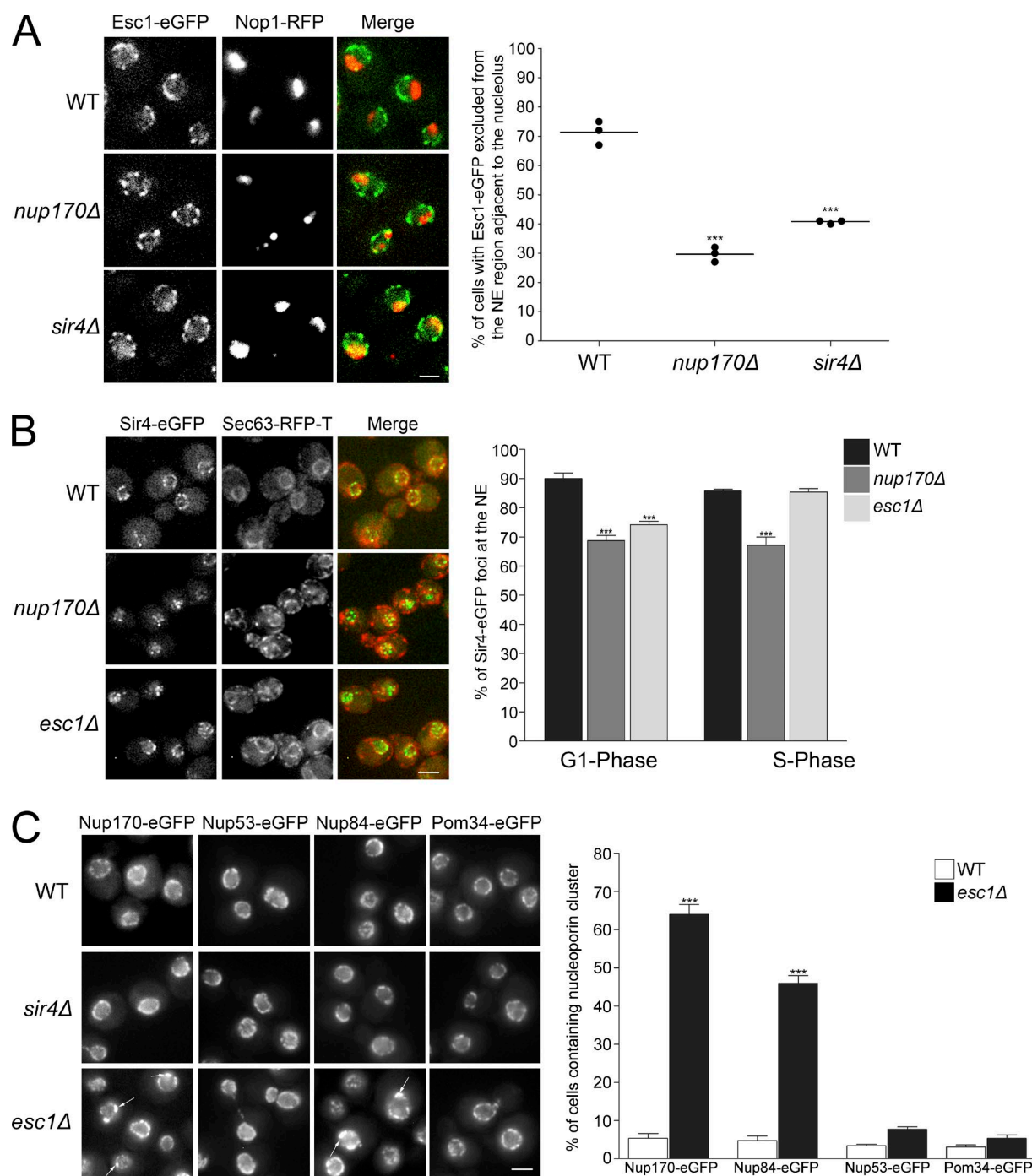
Figure 4. **Interdependence of Nup170, Esc1, and Sir4 on their respective subcellular distribution.** (A) WT, *nup170Δ*, and *sir4Δ* cells producing Esc1-eGFP and the nucleolar marker Nop1-RFP were examined by epifluorescence microscopy. Images of Esc1-eGFP, Nop1-RFP, and a merged image are shown. The number of cells in which the Esc1-eGFP signal was excluded from the NE adjacent to the nucleolar Nop1-RFP signal was determined and expressed as a percentage of the total number of cells examined. A scatter plot of data obtained from three biological replicates is shown. Data points for WT, *nup170Δ*, and *sir4Δ* were derived from 100 cells per experiment. (B) WT, *nup170Δ*, and *esc1Δ* cells producing Sir4-eGFP and the NE/ER marker Sec63-RFP-T were examined by epifluorescence microscopy. Images of Sir4-eGFP, Sec63-RFP-T, and a merged image are shown on the left. Using bud size to identify G1- and S-phase cells, the percentage of total Sir4-eGFP foci that overlaps with the NE/ER marker Sec63-RFP-T was determined (right). Bars represent the mean from three biological replicates. Error bars indicate SD. (C) Subcellular distribution of the indicated Nup-eGFP fusions in WT, *esc1Δ*, and *sir4Δ* cells was examined, and images were obtained. Arrows point to Nup170-eGFP and Nup84-eGFP clusters in *esc1Δ* cells. Quantification of the percentage of cells showing clusters is shown on the left (see Materials and methods). ***, $P \leq 0.001$. Error bars show SD. Bars, 2 µm.

cellular distribution of Nup170-eGFP or Sir4-eGFP (Fig. S3, A and B). Together, these results support the conclusion that Siz2 is part of a network of interacting proteins that includes Nup170, Sir4, and Esc1.

## Esc1 is bound to two separate Nup170-containing complexes

The physical association of Sir4, Esc1, Siz2, and Nup170 suggests that these proteins exist within one or more protein
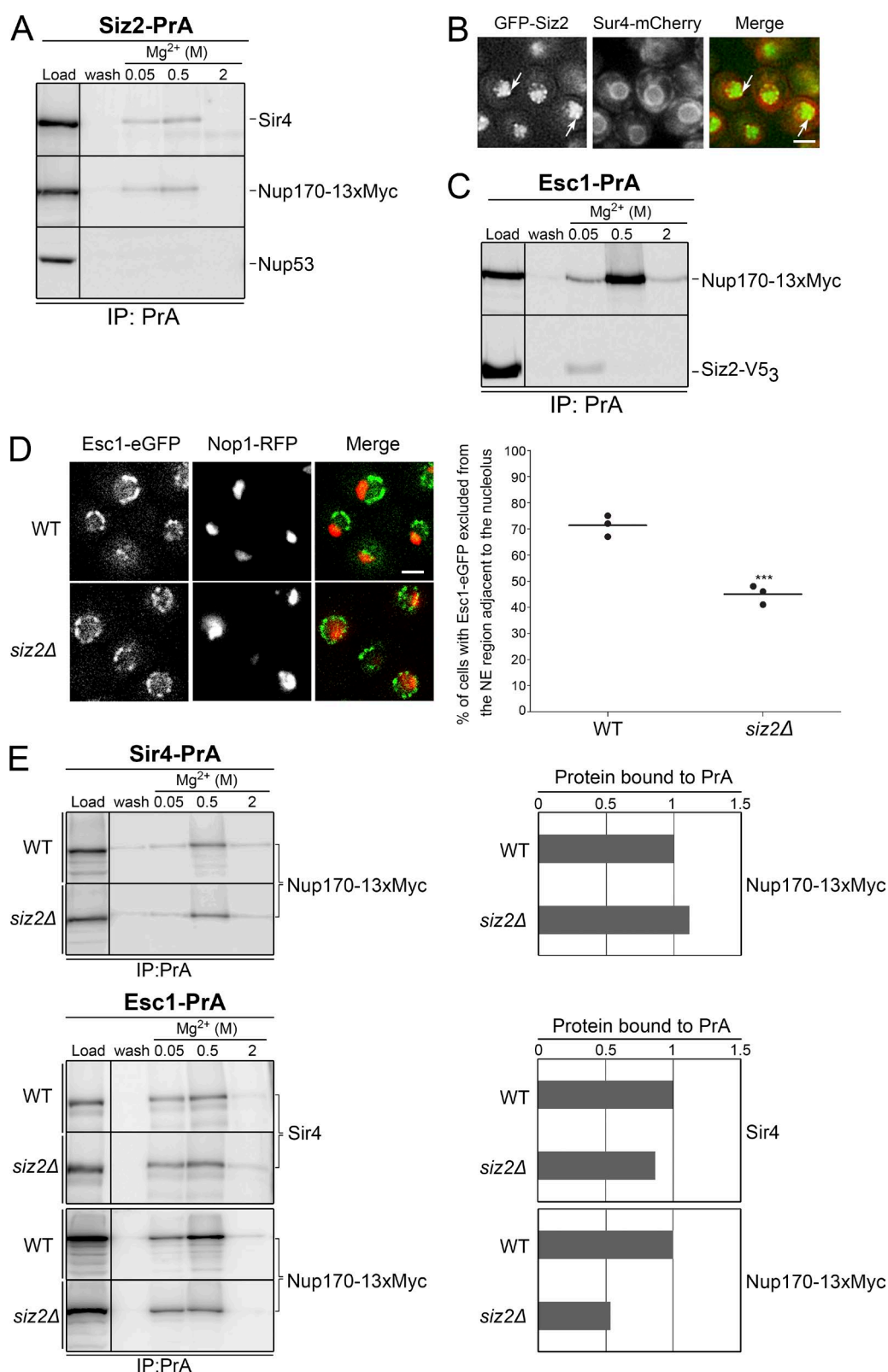
Figure 5. **Siz2 is associated with both Nup170 and Sir4.** (A) Siz2-PrA was affinity purified and analyzed by Western blotting as described in Fig. 2 to detect the indicated proteins. (B) Shown are images obtained by epifluorescence microscopy of GFP-Siz2 and Sur4-mCherry in WT cells. Arrows point to representative GFP-Siz2 foci at the NE. GFP-Siz2 foci at the nuclear periphery were highlighted using the unsharp mask function in ImageJ. (C) Esc1-PrA was affinity purified and analyzed by Western blotting as described in Fig. 2 to detect the indicated proteins. (D) Subcellular distribution of Esc1-eGFP relative to the nucleolar marker Nop1-RFP was assessed in WT and *siz2Δ* cells as described for Fig. 4 A. ***, P ≤ 0.001. (E) Sir4-PrA and Esc1-PrA were affinity purified from cell extracts of WT and *siz2Δ* deletion mutant strains and analyzed by Western blotting to detect the indicated proteins. To the right of the Western blots, the indicated proteins were quantified as described in Fig. 3. Additional biological replicates of these affinity purification experiments are shown in Fig. S1. Bars, 2 µm.
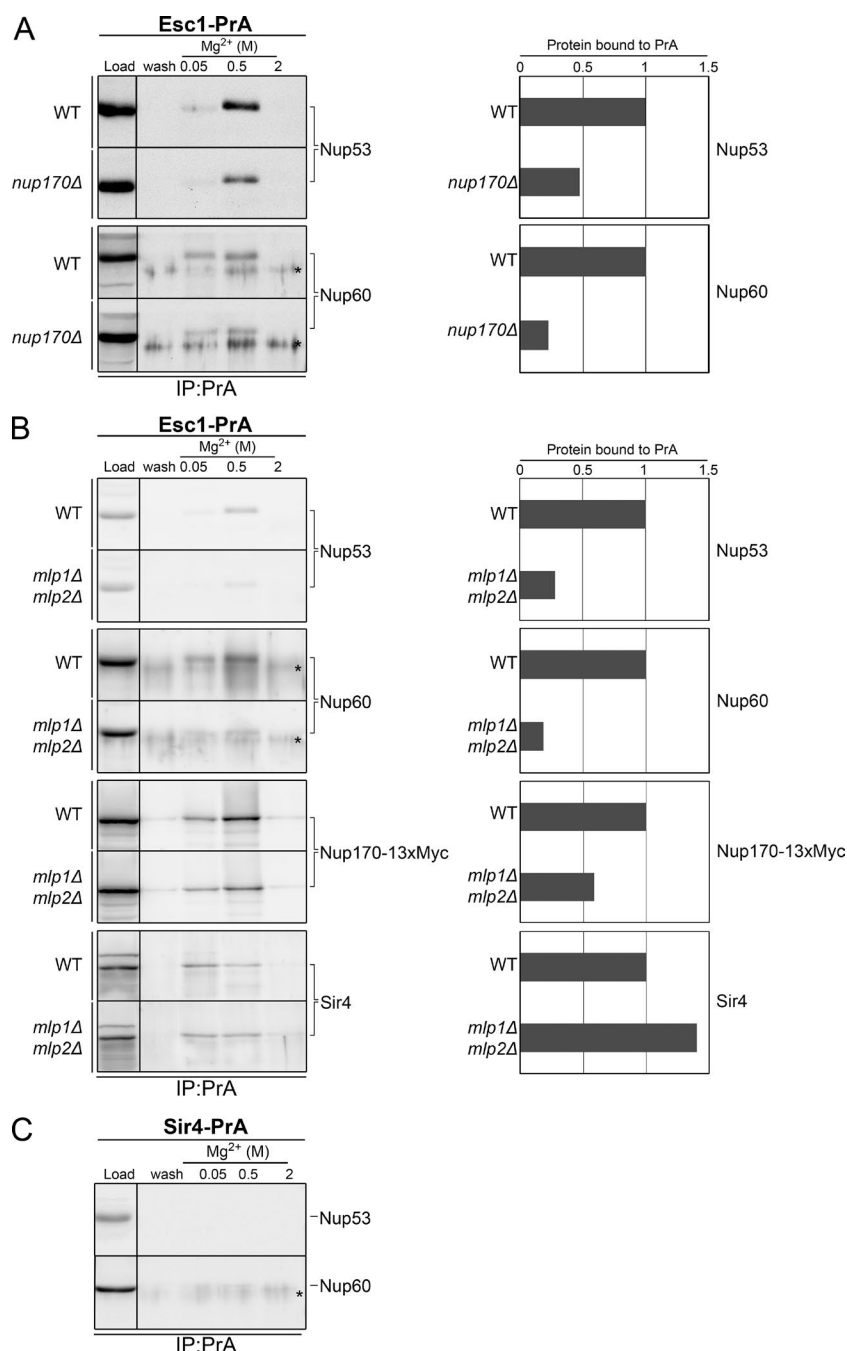
Figure 6. **Analysis of Esc1 and Sir4 interactions with Nups.** Esc1-PrA was affinity purified from cell extracts of WT, *nup170Δ* (A), and *mlp1Δ mlp2Δ* (B) strains and analyzed by Western blotting to detect the indicated proteins. To the right of the Western blots, the indicated proteins were quantified as described in Fig. 3. Asterisks shown in anti-Nup60 blots denote the position of a background band present in the wash and elution fractions. Note, additional biological replicates of the affinity purification experiments shown in these panels are presented in Fig. S1. (C) Sir4-PrA was affinity purified and analyzed by Western blotting as described in Fig. 2 to detect Nup53 and Nup60.

complexes at the NE. Because Nup170 is a structural component of NPCs, we further examined whether this complex is associated with NPCs. Previous fluorescence microscopy analysis has shown that Esc1 and Sir4 foci at the NE exhibit both overlapping and nonoverlapping signals with Nups (Andrulis et al., 2002; Taddei et al., 2004; Niepel et al., 2013). To better understand the physical relationships between these proteins and NPCs, we focused on further defining their interactions with a broader spectrum of Nups.

Esc1 has been reported to exhibit partial colocalization with FG-Nups using fluorescence microscopy analysis (Taddei et al., 2004). Moreover, two Nups, Nsp1 and Nup192, as well as the NPC-associated proteins Mlp1 and Mlp2, were detected bound to affinity-purified Esc1-PrA (Niepel et al., 2013). Because Nup170 and Nup192 are members of the inner rings

of the NPC and share binding partners (Alber et al., 2007a,b; Amlacher et al., 2011), we further analyzed the interactions of Esc1 with Nup170- and Nup192-interacting Nups. As shown in Fig. 6 A, Nup53, a direct binding partner of Nup170 and Nup192 (Lusk et al., 2002; Makio et al., 2009; Onischenko et al., 2009), and Nup60, a Nup positioned near Nup192 in the NPC (Alber et al., 2007a,b), were also detected in association with Esc1-PrA. Consistent with the association of Esc1 with an NPC subcomplex containing Nup170, the amount of Nup53 and Nup60 detected bound to Esc1-PrA was reduced in a strain lacking Nup170 (Figs. 6 A and S1 C).

Similar to what we observed in the absence of Nup170 (Fig. 4 A), the NE distribution of Esc1-GFP is altered in a strain lacking Mlp1 and Mlp2, leading Niepel et al. (2013) to suggest that these proteins, directly or indirectly, mediate Esc1 binding

to NPCs. We tested this idea by affinity-purifying Esc1-PrA from cells lacking Mlp1 and Mlp2. As shown in Fig. 6 B (also see Fig. S1 D), loss of the Mlp proteins reduced the amount of Nup53 and Nup60 that copurified with Esc1-PrA. These results are consistent with the conclusion that the Mlp proteins are required for the association of Esc1 with NPCs.

In contrast, the loss of the Mlps did not have a similar effect on the interactions of Esc1-PrA with Sir4 or Nup170. For example, the amount of Sir4 that copurified with Esc1-PrA derived from *mlp1Δmlp2Δ* cell extracts was similar to, or even slightly higher than, that observed using WT cell extracts (Figs. 6 B and S1 D). For Nup170, although the total amount of Nup170 copurifying with Esc1-PrA was reduced in the *mlp1Δmlp2Δ* mutant, consistent with the loss of Esc1 at NPCs, a significant proportion of Nup170 remained bound to Esc1. These observations are consistent with the presence of an Esc1/Nup170-containing complex that is resistant to the loss of the Mlp proteins and likely occurs outside of NPCs.

## Sir4 associates with a subset of scaffold Nups

As was previously shown (Van de Vosse et al., 2013) and confirmed here, Nup170 copurifies with Sir4-PrA (Figs. 2 C and 5 E), but this complex lacks at least two other Nups: Nup53, a direct binding partner of Nup170 within the NPC (Makio et al., 2009), and Nup60 (Fig. 6 C). Consistent with these results, affinity purification of Nup53-PrA or Nup60-PrA revealed little or no detectable Sir4 but a clear association with Nup170 (Fig. S4, A and B). Notably, because Nup60 does not appear to directly interact with Nup170 (Alber et al., 2007a,b), the presence of Nup170 and Nup53 in complex with Nup60-PrA suggests that bridged molecular interactions within NPCs are maintained under the conditions used here for complex isolation, as are the interactions between Nup170 and Nup53. These results led us to conclude that Sir4 interacts with a population of Nup170 that is not associated with Nup53 or Nup60, and thus, is distinct from holo-NPCs. As discussed above, our analysis of Sir4-PrA–associated proteins also detected Siz2. Importantly, purified Siz2-PrA was similarly associated with Sir4 and Nup170, but not Nup53 (Fig. 5 A). Because both Sir4 and Siz2 are also detected in association with Esc1, we envisage that these three proteins interact, directly or indirectly, with Nup170 in complexes distinct from holo-NPCs.

We next examined whether the complex of proteins containing Sir4, Siz2, and Esc1 was associated with Nup170 alone or with additional Nups. The latter scenario seemed likely, as Nup157 is associated with purified Sir4 (Van de Vosse et al., 2013) and Siz2 (Fig. S4 C). For this analysis, we focused on defining the broader spectrum of Nups associated with affinity-purified Sir4-PrA. Targeted Nups included those found within various substructural regions of the NPC, including members of the inner ring Nup170 complex (Nup170, Nup192, Nup157, Nup188, Nup53, Nup59, and Nic96), the outer ring Nup84 complex (Nup84, Nup133, and Nup145C), a pore membrane protein that directly binds Nup170 (Pom152; Makio et al., 2009; Onischenko et al., 2009), and Nups associated with the cytoplasmic (Gle1) and nucleoplasmic (Mlp1, Nup60, and Nup1) faces of the NPC (Rout et al., 2000; Hoelz et al., 2011). As shown in Fig. 7 B, Sir4-PrA specifically copurified with multiple components of the inner ring Nup170 subcomplex (Nup170, Nup192, Nup157, Nup188, and Nic96), each of the components of the outer ring examined (Nup84, Nup133,

and Nup145C), and Pom152. In contrast, several Nups showed little or no association with Sir4, including the inner ring proteins Nup53 and Nup59, and the various cytoplasmic (Gle1) and nucleoplasmic (Mlp1, Nup60, and Nup1) Nups examined. These results suggested the existence of a Snup complex separate from holo-NPCs.

We predicted that Nups associated with the Snup complex, such as Nup170 and Nup157, would exhibit a greater degree of colocalization with Sir4 than those absent from the Snup complex (e.g., Nup53). To test this, Sir4-eGFP foci positioned at the nuclear periphery were compared with those of various RFP-T–tagged Nups (Fig. 7 C). Examining different dual-tagged strains, we observed that NE-associated foci arising from Nup170-RFP-T, Nup157-RFP-T, or Nup84-RFP-T showed multiple foci that colocalized with Sir4-eGFP. Quantification of the frequency of overlap in optical sections revealed that ~65%, ~70%, and ~58% of Sir4-eGFP foci colocalize with Nup170-RFP-T, Nup157-RFP-T, and Nup84-RFP-T, respectively. In contrast, Nup53-RFP-T showed a significantly lower colocalization with Sir4-eGFP (~38%). Thus, Sir4p exhibits preferential colocalization with those Nups detected in the Snup complex.

## The Snup complex localizes to regions of the NE separate from NPCs

Our analysis of Nup copurification with Sir4 led us to conclude that Snup complexes are distinct from NPCs. On the basis of these results, we predicted that Nups present in both Snup complexes and NPCs (e.g., Nup170 and Nup157) would exhibit a higher level of colocalization compared with one another than compared with a Nup present only in NPCs, such as Nup53 or Nup60. To test this prediction, the localization of Nup170-RFP-T, as a component of both Snup complexes and NPCs, was compared with various eGFP-tagged Nups, and the percentage of Nup-eGFP signal that overlapped with Nup170-RFP-T at the nuclear periphery was quantified (see Materials and methods). First, we examined cells expressing both Nup170-eGFP and Nup170-RFP-T (i.e., a situation in which the fusion proteins are predicted to be similarly represented in Snup complexes and NPCs). We observed that ~78% of Nup170-eGFP colocalized with Nup170-RFP-T, suggesting that this represented the approximate maximum value for Nup-Nup colocalization that could be detected using our quantification procedure (Fig. 8 B, Nup170 [diploid cells]). The localization of Nup170-RFP-T was then compared with that of various eGFP-tagged Nups. As shown in Fig. 8, several Nups shown to copurify with Sir4, including Nup157, Nup188, Nic96, Nup84, and Nup145C (Fig. 8 B), uniformly exhibited a higher percentage (~70%) of overlap with Nup170-RFP-T than those Nups that did not bind Sir4, including Nup53, Nup59, and Nup60 (present in NPCs but not the Snup complex), which showed significantly lower colocalization with Nup170-RFP-T (~45%) and distinct regions of nonoverlapping Nup170-RFP-T (Fig. 8 A).

The results of our colocalization analysis suggested that a higher (~70%) or lower (~50%) level of overlap between Nup170 and another Nup directly correlated with the presence or absence of that Nup in the Snup complex. Therefore, we used the Nup170 colocalization analysis to assess the potential interactions of other Nups with the Snup complex, including several Nups that we were unable to evaluate by copurification with Sir4 because of nonspecific interactions with IgG-conjugated magnetic beads (not depicted). These included Nup82 and
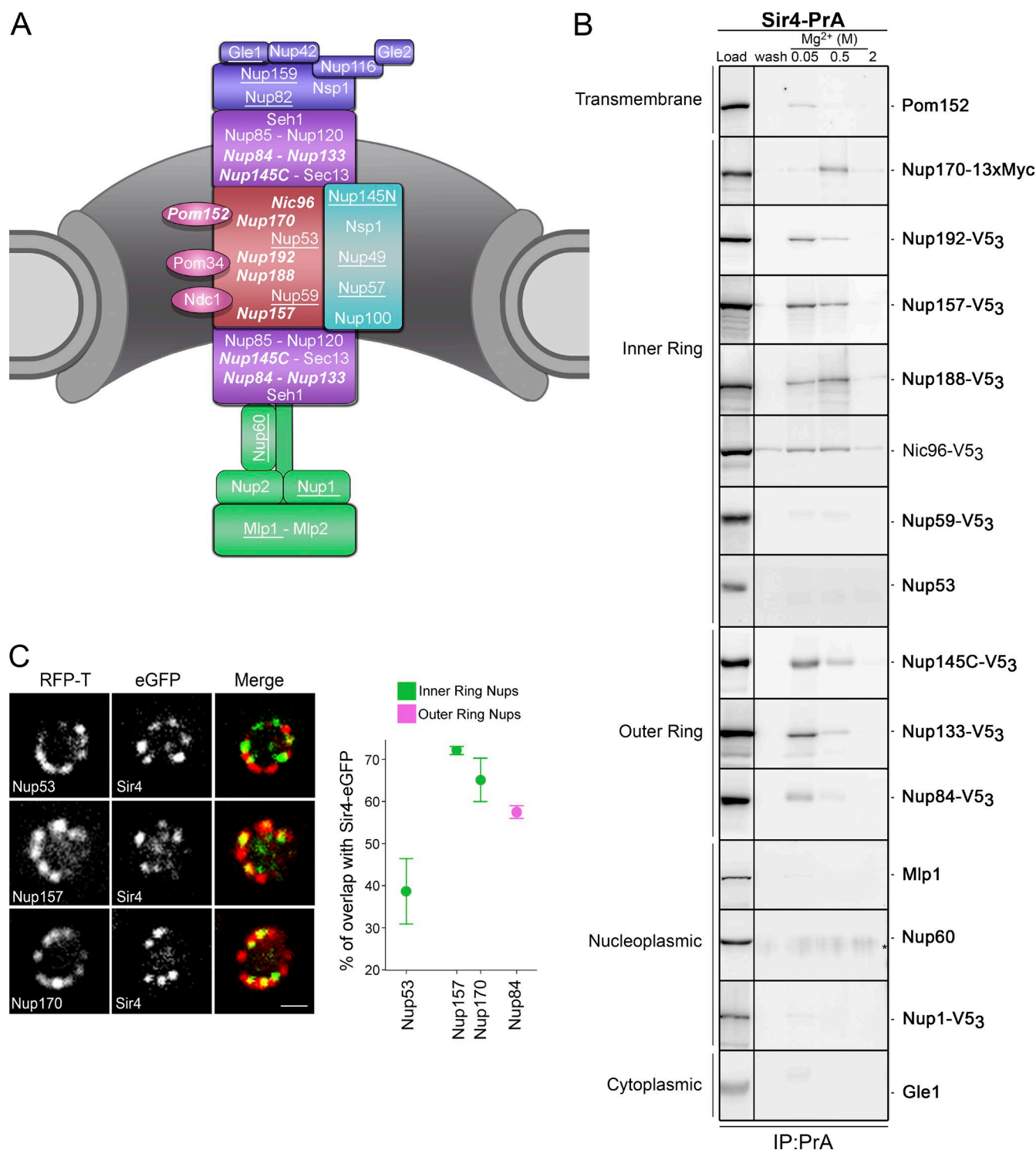
Figure 7. **Sir4 associates with inner and outer ring Nups.** (A) Shown is a schematic diagram of Nups present in various subcomplexes and their general location within a spoke of the NPC. Nups present in the Nup170-containing inner ring complex (red), the Nup84-containing outer ring complexes (purple), pore membrane Nups (magenta), central channel Nups (cyan), cytoplasmically positioned Nups, including the Nup82 complex (blue), and nucleoplasmic Nups (green) are shown (see Beck and Hurt, 2017). Note that Nups tested for their association with Sir4-pA (B) or colocalization with Nup170-RFP (Fig. 8) are underlined or italicized. The italicized Nups are proposed to be part of the SNUP complex and underlined Nups are not. (B) Coaffinity purifications were performed and analyzed by Western blotting using cell extracts from Sir4-PrA–producing strains also containing the indicated tagged Nups. Western blots for Pom152, Mlp1, Nup60, Nup53, and Gle1 were performed using samples from the Sir4-PrA/Nup170-13xMyc–producing strain and antibodies directed against the indicated proteins. The asterisk shown in the anti-Nup60 blot denotes the position of a background band present in the wash and elution fractions. Blots are grouped based on the general localization of the Nup (indicated on the left). (C) Epifluorescence microscopy images depicting the localization of Sir4-eGFP and Nup53-RFP-T, Nup157-RFP-T, or Nup170-RFP-T . Colocalization of the indicated pairs of fluorescent proteins was quantified as the percentage of total Sir4-eGFP foci ($n > 4500$) that overlap with the respective Nup-eGFP foci. Bars represent the mean of three biological replicates for each colocalization experiment. Error bars indicate SD. Bar, 1 µm.
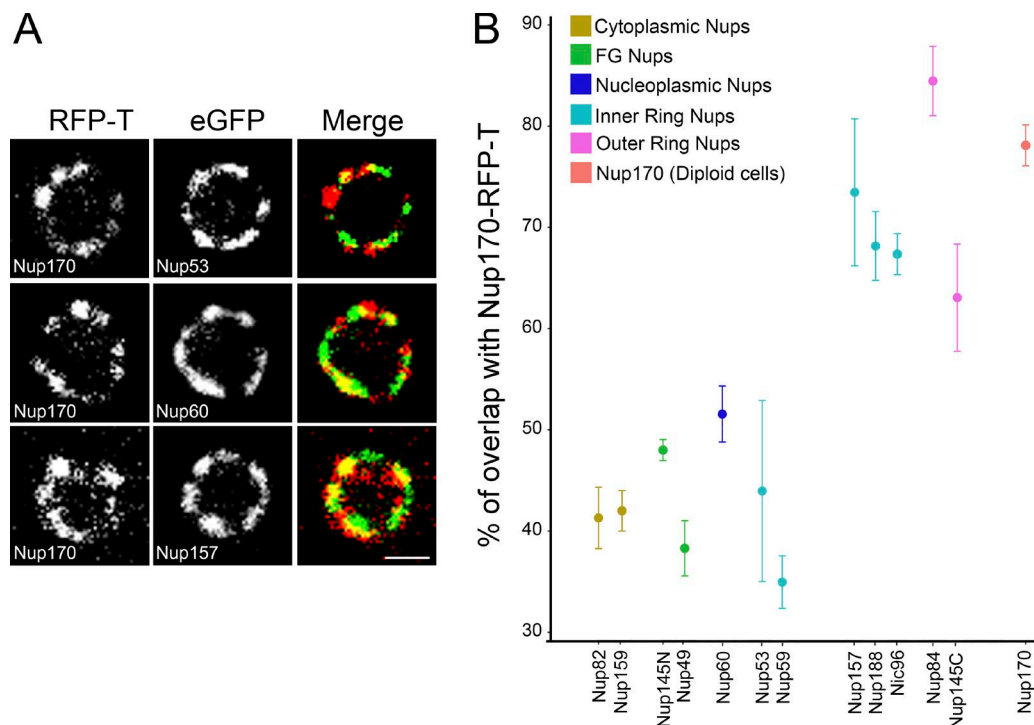
Figure 8. **Colocalization of Nups with the Snup component Nup170.** (A) Representative epifluorescence microscopy images depicting the colocalization of Nup170-RFP-T with Nup53-eGFP, Nup60-eGFP, and Nup157-eGFP. (B) Colocalization of the indicated pairs of fluorescent proteins was quantified as the percentage of total Nup170-RFP-T foci (y axis) that overlap with the indicted Nup-eGFP fusions (x axis). Note that we tested switching the tag on Nup170 to eGFP and analyzing Nup170-eGFP/Nup53-RFP-T and Nup170-eGFP/Nup157-RFP-T and the results were similar to those reported here for Nup170-RFP-T/Nup53-eGFP and Nup170-RFP-T/Nup157-eGFP (not depicted). Bars represent the mean of three biological replicates for each colocalization experiment. The number of foci examined in each biological replicate varied from ~4,000 to 10,000. Error bars indicate SD. Bar, 1 µm.

the FG-Nups Nup49, Nup145N, and Nup159. Each of these Nups showed levels of colocalization with Nup170 similar to Nups that are absent from the Snup complex, such as Nup53 (Fig. 8 B). Cumulatively, our data suggest that the Snup complex is composed of inner and outer ring Nups in a structure distinct from holo-NPCs.

## Discussion

The study of telomere and subtelomeric chromatin tethering to the NE has provided insights into the interactions of chromatin and the NE membrane and the significance of this association in determining chromatin structure and regulating gene expression. Numerous studies have identified multiple proteins that contribute to telomere tethering (Kupiec, 2014). However, in many instances the functional and physical relationships between these factors are ill-defined. In this study, we identified a network of interactions between a subset of proteins previously shown to contribute to telomere anchoring to the NE and gene silencing, including Sir4, Siz2, Esc1, and Nup170. Importantly, we demonstrate that, although Esc1 is associated with NPCs, and Nup170 is a constitutive component of this structure, their association with Sir4 and Siz2 occurs outside of fully assembled NPCs. Instead, Sir4 and Siz2 are bound to a complex consisting of Esc1, Nup170, and a subset of Nups that contribute to the core scaffold of the NPC, which we collectively term the Snup complex. On the basis of these and previous (Van de Vosse et al., 2013) functional and physical analyses, the Snup complex is proposed to contribute to subtelomeric chromatin structure and gene silencing.

The presence of Sir4, Esc1, Nup170, and Siz2 within a physical complex is consistent with accumulating data pointing to their shared functional properties. Foremost among these are their roles in the physical association of telomeres with the NE (Palladino et al., 1993; Andrulis et al., 2002; Ferreira et al., 2011; Van de Vosse et al., 2013). The association of telomeres with the NE is dependent on partially redundant pathways that use several NE-associated proteins including Mps3, Esc1, and Nup170 as tethering factors (Andrulis et al., 2002; Bupp et al., 2007; Van de Vosse et al., 2013). These proteins interact with telomeric and subtelomeric chromatin-associated proteins such as Sir4, yKu70/80, and Est1. Siz2 is also required for NE-association of telomeres, potentially functioning in this role through its SUMOylation of chromatin-associated Sir4 and yKu80 (Ferreira et al., 2011). Why these multiple tethering pathways exist is unclear, but a discriminating property of them is their role in telomere anchoring during different stages of the cell cycle, with most studies focusing on their telomere tethering capabilities during G1 and S phase. For example, Mps3, through its interactions with Sir4 and Est1, contributes to anchoring telomeres to the NE during S phase (Schober et al., 2009). In contrast, Nup170 is required for telomere tethering in G1 phase (Van de Vosse et al., 2013). Similarly, Esc1 also plays a role in G1-phase telomere tethering (Taddei et al., 2010). These functional distinctions between Nup170 and Mps3 place these proteins in distinct tethering pathways, which is consistent with our data showing that Nup170 and Esc1 are present in a complex that is physically distinct from Mps3 (Fig. 2).

Our data further place Esc1 and Nup170 in a complex with Sir4 (Fig. 2). These data are consistent with previous

publications separately reporting Sir4/Esc1 (Andrulis et al., 2002) and Sir4/Nup170 interactions (Van de Vosse et al., 2013). In the latter case, the proposed interaction between Nup170 and Sir4 was supported by ChIP-chip analysis that revealed the association of Nup170 with subtelomeric chromatin and the dependence of this binding on Sir4. As shown in Fig. 1, the binding of Nup170 to subtelomeric chromatin was not uniform but rather occurred within discrete regions, and a similar discontinuous pattern of Sir4 enrichment on subtelomeric chromatin was also observed by Ellahi et al. (2015). Remarkably, comparison of these two binding profiles shows extensive overlap (Fig. 1). These data, together with our observations that these proteins coaffinity purify (Fig. 2) and are detected in overlapping foci at the NE (Fig. 7), provide strong support for the existence of a chromatin-associated complex consisting of Nup170 and Sir4.

The chromatin-associated Sir4/Nup170 complex is also predicted to contain Esc1. In addition to their copurification (Fig. 2), various observations support the existence of a complex containing Sir4/Nup170/Esc1. First, the presence of all three of these proteins is required to maintain the integrity of this complex, and the loss of any one member alters the interaction of the remaining two (Fig. 3). Second, the normal NE distribution of these three proteins is interdependent on one another. For example, the loss of Esc1 or Nup170 leads to a decrease in the NE association of Sir4 (Fig. 4 B), whereas the loss of Nup170 or Sir4 alters the NE distribution of Esc1 (Fig. 4 A). Third, the functional consequences of the loss of any one of these three proteins are also shared, including defects in the silencing of genes positioned in subtelomeric chromatin regions and a decrease in the NE association of telomeres (Palladino et al., 1993; Andrulis et al., 2002; Van de Vosse et al., 2013; Fig. S5). These phenotypes are presumed to arise, at least in part, because of a failure of Sir4 to correctly load onto subtelomeric chromatin (Andrulis et al., 2002; Van de Vosse et al., 2013). These multiple observations lead us to conclude that the Snup complex plays a role in the structure and NE tethering of subtelomeric chromatin.

Both Sir4 binding partners, Nup170 and Esc1, are associated with NPCs. Nup170 is a well-established component of the inner ring scaffold of the NPC. Esc1 has been detected bound to NPC-associated proteins, including Nup192 and Mlp2, and fluorescence microscopy revealed partial colocalization of Esc1 with NPCs (Lewis et al., 2007; Niepel et al., 2013). Niepel et al. (2013) also showed that cells lacking the Mlp proteins exhibited an altered distribution of Esc1, suggesting that Mlp proteins may link Esc1 to NPCs. Here, we have further shown that several Nups, including Nup53, Nup60, and Nup170, are associated with affinity-purified Esc1 (Fig. 6 B). In addition, we observed that the loss of the Mlps reduces the amount of Nup53 and Nup60 associated with Esc1, providing further evidence for the role of the Mlp proteins in linking Esc1 to NPCs (Fig. 6 B). Notably, however, the absence of the Mlp proteins only partially decreased the levels of Nup170 associated with purified Esc1 and had no effect on the interaction of Esc1 with Sir4 (Fig. 6 B). A reasonable interpretation of this result is that a Nup170/Esc1/Sir-containing complex exists outside of NPCs and is unaffected by the loss of Mlp proteins.

Importantly, our analysis of affinity-purified Sir4 revealed its association with a distinct subset of Nups, which led us to hypothesize that these Nups were not part of NPCs, but rather a distinct complex. Through our examination of Nups bound to Sir4, we detected multiple proteins that contribute to the inner and outer ring complexes. Inner ring Nups included Nup170, Nup192, Nup157, Nup188, and Nic96, whereas those detected from the outer ring Nup84 complex included Nup84, Nup133, and Nup145C (Fig. 7). Also present was Pom152, a membrane protein that directly interacts with Nup170 (Makio et al., 2009; Onischenko et al., 2009). However, absent from the Sir4-associated proteins were various Nups such as Nup53, Nup59, Nup60, Nup1, and Mlp1 (Figs. 6 C and 7 B). These observations were striking, because this group included Nups (such as Nup53) that are direct binding partners of Nup170, Nic96, and Nup192 within the NPC (Makio et al., 2009; Amlacher et al., 2011), and when, for example, Nup53-PrA or Nup60-PrA are purified, Nup170 is readily detected (Fig. S4).

The affinity purificadion experiments we performed support the hypothesis that Snup complexes are physically distinct from NPCs. This idea was further supported by the results of fluorescence microscopy experiments comparing the localization of Nups present in Snups complexes with those that are not. Importantly, when we compared the localization of Nups present in both the Snup complex and NPCs, they showed a higher degree of colocalization with one another than with Nups present in only NPCs. For example, Nup157 and Nup170 (present in both NPCs and Snup complexes) showed significantly higher levels of colocalization (~73%) than that observed between Nup53 (absent from Snup complexes) and Nup170 (~44%; Fig. 8 A). This trend was consistently observed. When those Nups detected in the Snup complex (including Nup157, Nup188, Nic96, Nup84, and Nup145C) were compared with Nup170, they showed a higher degree of colocalization than those not detected in the Snup complex (Nup53, Nup59, and Nup60; Fig. 8 B). Based on the uniformity of these results, we used this assay to assess the interactions of additional Nups, including Nup82 and the FG-Nups Nup159, Nup145N, and Nup49. Each of these Nups showed lower levels of colocalization with Nup170, similar to that observed for Nup53, suggesting they are not present in the Snup complex.

Our localization data also revealed a higher degree of fluorescence colocalization between Sir4 and those Nups detected bound to Sir4 in our affinity purification experiments, including Nup170, Nup157, and Nup84 (Fig. 7 C). This is in contrast to Nup53, which is absent from the Snup complex. The existence of Snup complexes with distinct composition and localization from NPCs may provide insight into the reasons for conflicting studies on the association of telomeres with NPCs. On the basis of our data, Nups not associated with the Snup complex are predicted to exhibit only random levels of colocalization with telomere-associated Sir4. These results shed light on a previous study that Mlp proteins interact with telomeres (Galy et al., 2000), which was refuted in a later study (Hediger et al., 2002). Consistent with the latter study, we do not detect Mlps in association with the Snup complex (Fig. 7 B). Moreover, our results may also explain previous studies of minimal colocalization of Sir4 with Nup49-GFP (Taddei et al., 2004), as this Nup does not appear to be part of the Snup complex (Fig. 8 B).

The existence of the Snup complex raises many questions about its physical and functional relationship to NPCs. Although not all 30 yeast Nups have been examined, our initial characterization of the Snup complex described here (Fig. 7 B) reveals that its Nup components are largely contributed by members of the inner and outer ring complexes, whereas absent from the complex are Nups associated with the nucleoplasmic (Nup60, Mlp1, and Nup1) and cytoplasmic (Nup82, Nup159,

and Gle1) faces of the NPC and the central channel FG-Nup Nup49 (Fig. 8). Intriguingly, also not present in the Snup complex are Nup145N and the paralogs Nup53 and Nup59. Both Nup145N and Nup53 contain multiple interaction domains that allow them to bind several members of the inner ring complex, including Nup170 and Nup192 (Amlacher et al., 2011; Gaik et al., 2015). Nup53 has also been proposed to bridge Nup170 complexes of adjacent inner ring spokes (Lin et al., 2016). Considering the potential functions of these Nups, we assume the inner and outer ring components of the Snup complex are likely to form a structure related to, but distinct from, NPCs. Furthermore, additional compositional differences, including the lack of proteins functioning in mRNA and protein transport, also suggest that the Snup complex is unlikely to function in nuclear transport. Bearing in mind the functional data linking Nup170 to subtelomeric chromatin structure (Van de Vosse et al., 2013), it is plausible that Snup complex Nups function as a membrane-associated platform on which Sir4 and other factors are sequestered and rendered competent to interact with specific regions of subtelomeric chromatin.

The identification of Snup complexes also raises the question of their physical relationship to NPCs; for example, are they formed separately and represent distinct functional units, or are they temporally related to NPCs, perhaps representing an intermediate in NPC assembly capable of performing specific tasks before their maturation into NPCs? In the latter scenario, maturation of the Snup complex into a mature NPC would be predicted to suppress the chromatin-binding activity of Nup170 or other Snup complex Nups. Of note, a recent study reported results that support the idea that some Nups may mask or regulate the function of other Nups (Breuer and Ohkura, 2015). They showed in *Drosophila melanogaster* cells that an orthologue of yeast Nup170, Nup155, could mediate chromatin interactions with the NE. Importantly, this function of Nup155 could be repressed by other Nups, namely Nup62 and Nup93. We speculate that a similar masking event in yeast could regulate the accessibility of Nup170. In the absence of a masking event, a Nup170-containing Nup complex could bind Sir4 and contribute to the formation of the Snup complex, whereas the binding of masking Nups (with Nup53 representing a candidate) to the Nup170 complex could facilitate the maturation of the structure into an NPC.

Other observations also suggest that the Snup complex may transition between assembled and disassembled states during the cell cycle. This concept has its origins in observations that telomeres exhibit dynamic behavior during the cell cycle, being released from the NE for variable lengths of time during G1 and S phase, as well as late in S phase when telomeres replicate (Taddei and Gasser, 2012; Kupiec, 2014). Yeast Nups are not detected away from the NE; thus any release of telomeres from the NE is predicted to break this linkage. SUMOylation of telomere-associated proteins has been postulated to control their association with the NE. Supporting this idea, the association of telomeres with the NE is dependent on the SUMO ligase Siz2, which SUMOylates Sir4 and yKu80, and functionally interacts with Esc1 (Ferreira et al., 2011; Pasupala et al., 2012). Our results showing that Siz2 interacts with the Snup complex (Fig. 5, A and C; and Fig. S4 C) suggests that local Siz2-mediated SUMOylation may promote telomere association with the Snup complex. Conversely, removing this modification could contribute to the release of telomeres from the NE during the cell cycle. It is intriguing to note that the desumoylase Ulp1 is associated with the nuclear baskets of NPCs. Thus, although Snup complexes containing Siz2 are predicted to promote an environment conducive to SUMOylation, NPC-associated Ulp1 is expected to promote deSUMOylation. The downstream consequences of the positioning of these SUMO regulators are envisaged to be the establishment of protein–protein interactions that support the binding of Snup complexes to subtelomeric chromatin, while inhibiting interactions with NPCs.

## Materials and methods

### Yeast strains and plasmids

Yeast strains used in this study are listed in Table S1. Cells were grown in YPD (1% yeast extract, 2% Bacto Peptone, and 2% glucose) or synthetic complete (SC) medium containing 2% glucose. Cultures were incubated at 30°C with constant agitation to mid-log phase ($OD_{600}$ 0.3–1.0) before harvesting. Transformations were performed using the lithium acetate/polyethylene glycol method (Gietz and Woods, 2002). Protein fusions were produced by modifying endogenous genes using a plasmid/PCR-based one-step genomic integration method (Longtine et al., 1998). Plasmids used in this study are listed in Table S2. pTM1198 was made by modifying the plasmid pFA6-GFP(S65T)-kanMX6 (Longtine et al., 1998), wherein the coding sequence for *GFP(S65T)*, bounded by the Pac1 and Asc1 restriction enzyme sites, was replaced by the coding sequence for $V5_3$, using the same restriction enzyme sites. pSIZ2pr-GFP was made by modifying the plasmid pFA6-HisMX6-PGAL1-GFP (Longtine et al., 1998), wherein the *GAL1* promoter sequence, bounded by the Bgl-II and Pac1 restriction enzyme sites, was replaced by the *SIZ2* promoter sequence, using the same restriction enzyme sites.

Using plating assays, we examined the growth characteristics of the RFP-T and eGFP fusion strains as well as the various PrA fusion strains used in this study. We find that these strains show no growth defect relative to WT (BY4741) cells at both 30°C and 37°C as determined by colony size using plating assays. One exception was the Sir4-PrA/Nup170-13xMyc/Nup145C-$V5_3$ strain, which showed slightly smaller colony size.

### Coaffinity purification

Coaffinity purifications were performed using a procedure similar to that previously described (Van de Vosse et al., 2013). Cultures of cells producing a PrA or TAP fusion protein were grown overnight in 2 liters of YPD media to a final $OD_{600}$ of ∼1.0, then harvested by centrifugation. Cell pellets were washed twice with 500 ml water and once with 250 ml washing buffer (20 mM Hepes buffer, pH 7.4, 110 mM potassium acetate, and 2 mM magnesium chloride). The final cell pellet was extruded through a syringe directly into liquid nitrogen to flash-freeze the cells. The resulting "noodles" were subjected to seven rounds of planetary ball mill grinding (Reitch PM100; 2 min, 600 rpm per round), keeping the grinding vessel cold between rounds by partial emersion in $N_2$(l), yielding 1.0–2.0 g cell powder. 1.0 g cell powder was suspended in 2 ml lysis buffer (20 mM Hepes buffer, pH 7.4, 110 mM potassium acetate, 2 mM magnesium chloride, 0.1% Tween-20, antifoam-B emulsion [1:5,000], and protease inhibitor cocktail [complete EDTA-free pellets; 2 pellets/50 ml buffer; Roche]), and the resulting suspension was incubated on ice for 30 min, with vortexing every 5 min, to produce the cell lysate. The lysate was cleared by centrifugation at 1500 *g* for 10 min at 4°C. To the cleared lysate, IgG-conjugated magnetic beads (Dynabeads; Invitrogen) were added at a concentration of 3 mg beads/2 ml lysate, and the mixture was incubated for 1 h at 4°C with rotation. Beads were removed from the mixture using a magnet and

washed 10 times with lysis buffer at 4°C. Proteins bound to the beads were eluted at 4°C using 0.5 ml IP buffer (20 mM Hepes buffer, pH 7.4, 0.1% Tween-20, antifoam-B emulsion [1:5,000], and protease inhibitor cocktail) containing incrementally increasing concentrations of $MgCl_2$ (0.05, 0.5, and 2 M) followed by a final elution using 0.5 ml of 0.5 M acetic acid to release the PrA or TAP fusion protein from the beads. Samples from the cleared lysates (load) and the last wash (wash), as well as entire eluate samples, were subjected to TCA precipitation, and the resulting pellets were lyophilized in a CentriVap Centrifugal Vacuum (Labconco) and solubilized in 1× sample buffer for SDS-PAGE and Western blot analysis.

## Immunoblotting

Proteins were separated using SDS-PAGE and transferred to nitrocellulose membranes. Membranes were then incubated in blocking buffer (PBS containing 0.1% Tween-20 and 5% milk powder) for at least 1 h at room temperature. The blocking buffer was removed and replaced with fresh blocking buffer supplemented with an appropriate primary antibody, followed by incubation overnight at 4°C. Primary antibodies used are listed in Table S3. Membranes were washed three times using 0.1% Tween-20 in PBS and then incubated in blocking buffer supplemented with an appropriate secondary antibody–HRP conjugate (Bio-Rad) at 1:10,000 dilution for at least 1 h at room temperature. Membranes were washed three times using 0.1% Tween-20 in PBS. To visualize protein bands by chemiluminescence, membranes were incubated in ECL solution (Amersham) for at least 1 min then scanned using an ImageQuant LAS 4000 (GE) imaging system.

## Protein quantification

Levels of proteins copurifying with selected PrA fusions in WT and deletion mutants were compared (see Figs. 2, 4, and 5). PrA fusions were affinity purified from WT and mutant strains in parallel and under identical conditions. Fractions were analyzed simultaneously by Western blotting. Images of scanned membranes were analyzed using ImageQuant software (GE) to determine total pixel intensities (TPIs) of the interacting species present in the 0.05-, 0.5-, and 2-M $Mg^{2+}$ elution fractions. The sum total of pixels from the three samples, minus background pixels, yielded a TPI for the interacting protein ($TPI_{IP}$) examined. Western blot analysis was also used to determine the TPIs of the bound PrA fusion ($TPI_{PrA}$). The amount of the interacting protein eluted relative to the amount of PrA bound to beads was then determined by calculating the $TPI_{IP}/TPI_{PrA}$ ratio. These values were then scaled such that the relative amount of interacting protein that copurified with the PrA fusion ($TPI_{IP}/TPI_{PrA}$ ratio) derived from WT cells was set at 1.0. The $TPI_{IP}/TPI_{PrA}$ ratio from the deletion mutant cell extract was expressed as a ratio relative to WT. Note that Western analysis of total cell extracts from WT and mutants cells revealed no detectable difference in the cellular levels of the PrA fusions.

## Live-cell image acquisition

All cells used for live-cell imaging were grown in YPD liquid culture to an $OD_{600}$ ~0.5. Cells were harvested, washed once with SC medium, pelleted, and suspended in a small volume of SC medium to ~$10^6$ cells/µl. Before imaging, 1.5 µl cell suspension was spotted onto a microscope slide coated with a 2% agarose pad. Epifluorescence images were acquired using an Axio Observer.Z1 microscope (Zeiss) equipped with an UPlanS-Apochromat 100×/1.40-NA oil objective lens (Zeiss) and an AxioCam MRm digital camera with a charge-coupled device (Zeiss). Images showing (a) Esc1-eGFP/Nop1-RFP in WT and deletion strains, (b) various Nup-eGFP fusions in WT, *esc1Δ*, and *sir4Δ* strains, and (c) GFP-Siz2 were collected in a single focal plane through the center of nuclei. Images showing (a) Sir4-eGFP/Sec63-

RFP-T and (b) various eGFP/Tag-RFP-T combinations for colocalization were collected as 12 to 18 consecutive 0.2-µm stacks in the *z* axis. Images were saved using AxioVision software and rendered using ImageJ software (NIH) for display.

## Image analysis

To quantify the percentage of cells in which Esc1-eGFP was excluded from regions of the NE abutting the nucleolus, only those cells in which the Esc1-eGFP and Nop1-RFP signals were clearly visible in the focal plane of the acquired image were counted. Images were deconvolved using the nearest neighbor function of the AxioVision software deconvolution module (Zeiss) and rendered using ImageJ. Those cells in which the Esc1-eGFP signal was excluded from regions of the NE abutting the nucleolus and those cells that showed a clear localization at the NE adjacent to the nucleolus were counted. The percentage of the total cells showing exclusion was plotted.

Sir4-eGFP foci that localized at the NE in WT and various deletion mutant (*nup170Δ*, *esc1Δ*, *siz2Δ*) strains were defined by their colocalization with the NE/ER marker Sec63-RFP-T. Cells producing the Sir4-eGFP and Sec63-RFP-T fusions were acquired as 12–18 consecutive 0.2-µm stacks in the *z* axis. Images were deconvolved using the nearest neighbor function of the AxioVision software deconvolution module and rendered using ImageJ. Distinct Sir4-eGFP foci were counted, and grouped as either colocalizing, where complete or partial signal overlap was observed between Sir4-eGFP and Sec63-RFP-T, or not colocalizing, where no signal overlap was observed between Sir4-eGFP and Sec63-RFP-T. Percent colocalization was then expressed as the number of colocalizing Sir4-eGFP foci divided by the total number of Sir4-eGFP foci examined, and these values were plotted on a bar graph. Error bars shown indicate SD.

The presence of Nup-eGFP clusters in the *esc1Δ* mutant was quantified as follows. WT and *esc1Δ* cells producing the indicated Nup-eGFP fusion were acquired as 12–18 consecutive 0.2-µm stacks in the *z* axis. Midplane stacks through the nuclei of 50 different cells were isolated in a square region comprising 50 by 50 pixels. 3D pixel signal intensity maps of the selected squares were created using the ImageJ plugin Interactive 3D Surface Plot, and the luminescence intensities of these pixels were plotted as peaks. We visually determined the mean peak heights representing the pixel intensity emitted by the Nup-eGFP protein. Nuclei were scored as containing clusters if they contained one or more peaks with greater than twice the mean pixel intensity of the remaining peaks in the optical section. GFP-Siz2 images were filtered using the unsharp mask function (radius [sigma], 3.0 pixels; mask weight, 0.8) of ImageJ, to differentiate signals at the nucleus edge from the more uniform nucleoplasmic signal.

Images of eGFP and Tag-RFP-T fusions used for colocalization of Sir4-eGFP with Nup-Tag-RFP-T and Nup-eGFP with Nup-Tag-RFP-T were acquired as 12–18 consecutive 0.2-µm stacks in the *z* axis. Images were deconvolved using the nearest neighbor function of the AxioVision software deconvolution module. Images were then rendered in ImageJ using a custom macro (Capitanio, 2016) to separate specific channels before importing processed images into Matlab (MathWorks). The following procedures were used to quantify the colocalization of eGFP and Tag-RFP-T signals (Figs. 7 and 8). Matlab was used to automate the detection, counting, and localization of signals along the nuclear periphery for each fluorescent protein. Using the Aro script (Matlab), previously described by Wu and Rifkin (2015) and adapted as described in Capitanio (2016), potential eGFP and Tag-RFP-T foci were first identified through local intensity maxima within the image. These putative foci were then submitted to a user-trained, supervised random forest classifier to identify "true" foci that exhibited a defined pixel intensity/area. These positively identified foci, for each

fluorescent protein fusion, were then plotted onto a 3D representation of the NE. The number of overlapping eGFP and Tag-RFP-T foci (foci were defined as overlapping when the distance between the maximum intensity pixel within the two separate foci was less than 300 nm or 5 pixels) was expressed as a percentage of the total number of eGFP or Tag-RFP-T foci identified (as indicated in the figure). All colocalization experiments were performed using three biological replicates. Averages of these replicates were graphed, and error bars for SD are shown.

### Comparison of Sir4 ChIP-Seq and Nup170 ChIP chip data

The Sir4 ChIP-Seq data were obtained from Ellahi et al. (2015), deposited in the NCBI Sequence Read Archive under accession no. SRP034921. Analysis was performed using Galaxy (https://usegalaxy.org/). Duplicated reads were removed using Trimmomatic (Bolger et al., 2014). Reads were mapped to sacCer1 genome using Bowtie2 (Langmead and Salzberg, 2012). Data normalization and per-base read counts were determined using deeptools2 (Ramírez et al., 2016). We determined enrichment using deeptools2 by dividing the IP reads by the input reads for every 5 bp. The Nup170 ChIP-chip data were obtained from Van de Vosse et al. (2013), deposited in NCBI Genome Expression Omnibus under accession no. GSE36794. The plotted Nup170 values represent the fold enrichment determined by comparing the IP and input samples for bound probes with a p-value ≤ 0.05. Data were compared and visualized using the Integrative Genomics Viewer application.

### Subnuclear localization of telomere 14-L

Yeast cells containing the LacO repeat inserted into Tel14-L at the locus ARS1413 as previously described (Taddei and Gasser, 2004), which also produce the LacO interactor Lac-I-GFP, were grown in YPD medium. Before imaging, cells were washed twice with SC medium and immobilized on 2% agarose pads. Telomere position inside the nucleus was determined relative to the NE marker Sec63-eGFP as previously described (Van de Vosse et al., 2013). Only the telomere present in the stack containing the brightest foci was counted. Telomere subnuclear localization was determined by dividing the telomere distance from the NE (TD) by the nuclear radius ($r$). The TD/$r$ ratio (R) was used to group telomeres into three concentric zones of equal area. Zone 1 represents foci with ratios ≤0.184 × R; zone 2 foci with ratios >0.184 × R and <0.422 × R; and zone 3 represents foci with ratios ≥0.422 × R.

### Online supplemental material

Fig. S1 shows the biological replicates of coaffinity purification experiments presented in Figs. 3, 5 E, and 6 (A and B). These experiments support the reproducibility of the coaffinity purification studies. Fig. S2 shows that the subcellular distribution of Mlp1 and Mlp2 is not altered in the *nup170Δ* cells. Fig. S3 shows the subcellular distribution of Sir4-eGFP, Nup53-eGFP, and Nup170-eGFP in asynchronously growing WT and *siz2Δ* cells. Fig. S4 shows the results of coaffinity purification experiments demonstrating that Nup60-TAP and Nup53-TAP interact with Nup170-13xMyc, and Siz2-PrA interacts with Nup157-V5₃. Fig. S5 shows that telomere tethering to the NE is altered in cells lacking selected proteins present in the Snup complex. Yeast strains, plasmids, and primary antibodies used in this study are listed in Tables S1, S2, and S3, respectively.

## References

Aitchison, J.D., and M.P. Rout. 2012. The yeast nuclear pore complex and transport through it. *Genetics.* 190:855–883. http://dx.doi.org/10.1534/genetics.111.127803

Alber, F., S. Dokudovskaya, L.M. Veenhoff, W. Zhang, J. Kipper, D. Devos, A. Suprapto, O. Karni-Schmidt, R. Williams, B.T. Chait, et al. 2007a. Determining the architectures of macromolecular assemblies. *Nature.* 450:683–694. http://dx.doi.org/10.1038/nature06404

Alber, F., S. Dokudovskaya, L.M. Veenhoff, W. Zhang, J. Kipper, D. Devos, A. Suprapto, O. Karni-Schmidt, R. Williams, B.T. Chait, et al. 2007b. The molecular architecture of the nuclear pore complex. *Nature.* 450:695–701. http://dx.doi.org/10.1038/nature06405

Amlacher, S., P. Sarges, D. Flemming, V. van Noort, R. Kunze, D.P. Devos, M. Arumugam, P. Bork, and E. Hurt. 2011. Insight into structure and assembly of the nuclear pore complex by utilizing the genome of a eukaryotic thermophile. *Cell.* 146:277–289. http://dx.doi.org/10.1016/j.cell.2011.06.039

Andrulis, E.D., D.C. Zappulla, A. Ansari, S. Perrod, C.V. Laiosa, M.R. Gartenberg, and R. Sternglanz. 2002. Esc1, a nuclear periphery protein required for Sir4-based plasmid anchoring and partitioning. *Mol. Cell. Biol.* 22:8292–8301. http://dx.doi.org/10.1128/MCB.22.23.8292-8301.2002

Beck, M., and E. Hurt. 2017. The nuclear pore complex: Understanding its function through structural insight. *Nat. Rev. Mol. Cell Biol.* 18:73–89. http://dx.doi.org/10.1038/nrm.2016.147

Bolger, A.M., M. Lohse, and B. Usadel. 2014. Trimmomatic: A flexible trimmer for Illumina sequence data. *Bioinformatics.* 30:2114–2120. http://dx.doi.org/10.1093/bioinformatics/btu170

Breuer, M., and H. Ohkura. 2015. A negative loop within the nuclear pore complex controls global chromatin organization. *Genes Dev.* 29:1789–1794. http://dx.doi.org/10.1101/gad.264341.115

Bupp, J.M., A.E. Martin, E.S. Stensrud, and S.L. Jaspersen. 2007. Telomere anchoring at the nuclear periphery requires the budding yeast Sad1-UNC-84 domain protein Mps3. *J. Cell Biol.* 179:845–854. http://dx.doi.org/10.1083/jcb.200706040

Capitanio, J.S. 2016. Github - ImageJ Script. https://github.com/jucapitanio/Software/tree/master/ImageJ macros/smFISH (accessed September 9, 2016).

Conrad, M.N., C.Y. Lee, G. Chao, M. Shinohara, H. Kosaka, A. Shinohara, J.A. Conchello, and M.E. Dresser. 2008. Rapid telomere movement in meiotic prophase is promoted by NDJ1, MPS3, and CSM4 and is modulated by recombination. *Cell.* 133:1175–1187. http://dx.doi.org/10.1016/j.cell.2008.04.047

Czapiewski, R., M.I. Robson, and E.C. Schirmer. 2016. Anchoring a leviathan: How the nuclear membrane tethers the genome. *Front. Genet.* 7:82. http://dx.doi.org/10.3389/fgene.2016.00082

Denison, C., A.D. Rudner, S.A. Gerber, C.E. Bakalarski, D. Moazed, and S.P. Gygi. 2005. A proteomic strategy for gaining insights into protein sumoylation in yeast. *Mol. Cell. Proteomics.* 4:246–254. http://dx.doi.org/10.1074/mcp.M400154-MCP200

Ebrahimi, H., and A.D. Donaldson. 2008. Release of yeast telomeres from the nuclear periphery is triggered by replication and maintained by suppression of Ku-mediated anchoring. *Genes Dev.* 22:3363–3374. http://dx.doi.org/10.1101/gad.486208

Ellahi, A., D.M. Thurtle, and J. Rine. 2015. The chromatin and transcriptional landscape of native *Saccharomyces cerevisiae* telomeres and subtelomeric domains. *Genetics.* 200:505–521. http://dx.doi.org/10.1534/genetics.115.175711

Ferreira, H.C., B. Luke, H. Schober, V. Kalck, J. Lingner, and S.M. Gasser. 2011. The PIAS homologue Siz2 regulates perinuclear telomere position and telomerase activity in budding yeast. *Nat. Cell Biol.* 13:867–874. http://dx.doi.org/10.1038/ncb2263

Gaik, M., D. Flemming, A. von Appen, P. Kastritis, N. Mücke, J. Fischer, P. Stelter, A. Ori, K.H. Bui, J. Baßler, et al. 2015. Structural basis for assembly and function of the Nup82 complex in the nuclear pore scaffold. *J. Cell Biol.* 208:283–297. http://dx.doi.org/10.1083/jcb.201411003

Galy, V., J.C. Olivo-Marin, H. Scherthan, V. Doye, N. Rascalou, and U. Nehrbass. 2000. Nuclear pore complexes in the organization of silent telomeric chromatin. *Nature.* 403:108–112. http://dx.doi.org/10.1038/47528

Gietz, R.D., and R.A. Woods. 2002. Transformation of yeast by lithium acetate/single-stranded carrier DNA/polyethylene glycol method. *Methods Enzymol.* 350:87–96. http://dx.doi.org/10.1016/S0076-6879(02)50957-5

Gilson, E., and V. Géli. 2007. How telomeres are replicated. *Nat. Rev. Mol. Cell Biol.* 8:825–838. http://dx.doi.org/10.1038/nrm2259

Gonzalez-Sandoval, A., and S.M. Gasser. 2016. On TADs and LADs: Spatial control over gene expression. *Trends Genet.* 32:485–495. http://dx.doi.org/10.1016/j.tig.2016.05.004

Gotta, M., T. Laroche, A. Formenton, L. Maillet, H. Scherthan, and S.M. Gasser. 1996. The clustering of telomeres and colocalization with Rap1, Sir3, and Sir4 proteins in wild-type *Saccharomyces cerevisiae*. *J. Cell Biol.* 134:1349–1363. http://dx.doi.org/10.1083/jcb.134.6.1349

Hannan, A., N.M. Abraham, S. Goyal, I. Jamir, U.D. Priyakumar, and K. Mishra. 2015. Sumoylation of Sir2 differentially regulates transcriptional silencing in yeast. *Nucleic Acids Res.* 43:10213–10226.

Hediger, F., K. Dubrana, and S.M. Gasser. 2002. Myosin-like proteins 1 and 2 are not required for silencing or telomere anchoring, but act in the Tel1 pathway of telomere length control. *J. Struct. Biol.* 140:79–91. http://dx.doi.org/10.1016/S1047-8477(02)00533-6

Hoelz, A., E.W. Debler, and G. Blobel. 2011. The structure of the nuclear pore complex. *Annu. Rev. Biochem.* 80:613–643. http://dx.doi.org/10.1146/annurev-biochem-060109-151030

Huh, W.K., J.V. Falvo, L.C. Gerke, A.S. Carroll, R.W. Howson, J.S. Weissman, and E.K. O'Shea. 2003. Global analysis of protein localization in budding yeast. *Nature.* 425:686–691. http://dx.doi.org/10.1038/nature02026

Kupiec, M. 2014. Biology of telomeres: Lessons from budding yeast. *FEMS Microbiol. Rev.* 38:144–171. http://dx.doi.org/10.1111/1574-6976.12054

Langmead, B., and S.L. Salzberg. 2012. Fast gapped-read alignment with Bowtie 2. *Nat. Methods.* 9:357–359. http://dx.doi.org/10.1038/nmeth.1923

Lewis, A., R. Felberbaum, and M. Hochstrasser. 2007. A nuclear envelope protein linking nuclear pore basket assembly, SUMO protease regulation, and mRNA surveillance. *J. Cell Biol.* 178:813–827. http://dx.doi.org/10.1083/jcb.200702154

Lin, D.H., T. Stuwe, S. Schilbach, E.J. Rundlet, T. Perriches, G. Mobbs, Y. Fan, K. Thierbach, F.M. Huber, L.N. Collins, et al. 2016. Architecture of the symmetric core of the nuclear pore. *Science.* 352:aaf1015. http://dx.doi.org/10.1126/science.aaf1015

Longtine, M.S., A. McKenzie III, D.J. Demarini, N.G. Shah, A. Wach, A. Brachat, P. Philippsen, and J.R. Pringle. 1998. Additional modules for versatile and economical PCR-based gene deletion and modification in *Saccharomyces cerevisiae*. *Yeast.* 14:953–961. http://dx.doi.org/10.1002/(SICI)1097-0061(199807)14:10<953::AID-YEA293>3.0.CO;2-U

Luo, K., M.A. Vega-Palas, and M. Grunstein. 2002. Rap1-Sir4 binding independent of other Sir, yKu, or histone interactions initiates the assembly of telomeric heterochromatin in yeast. *Genes Dev.* 16:1528–1539. http://dx.doi.org/10.1101/gad.988802

Lusk, C.P., T. Makhnevych, M. Marelli, J.D. Aitchison, and R.W. Wozniak. 2002. Karyopherins in nuclear pore biogenesis: A role for Kap121p in the assembly of Nup53p into nuclear pore complexes. *J. Cell Biol.* 159:267–278. http://dx.doi.org/10.1083/jcb.200203079

Makio, T., L.H. Stanton, C.C. Lin, D.S. Goldfarb, K. Weis, and R.W. Wozniak. 2009. The nucleoporins Nup170p and Nup157p are essential for nuclear pore complex assembly. *J. Cell Biol.* 185:459–473. http://dx.doi.org/10.1083/jcb.200810029

Marcomini, I., and S.M. Gasser. 2015. Nuclear organization in DNA end processing: Telomeres vs double-strand breaks. *DNA Repair (Amst.).* 32:134–140. http://dx.doi.org/10.1016/j.dnarep.2015.04.024

Niepel, M., K.R. Molloy, R. Williams, J.C. Farr, A.C. Meinema, N. Vecchietti, I.M. Cristea, B.T. Chait, M.P. Rout, and C. Strambio-De-Castillia. 2013. The nuclear basket proteins Mlp1p and Mlp2p are part of a dynamic interactome including Esc1p and the proteasome. *Mol. Biol. Cell.* 24:3920–3938. http://dx.doi.org/10.1091/mbc.E13-07-0412

Onischenko, E., L.H. Stanton, A.S. Madrid, T. Kieselbach, and K. Weis. 2009. Role of the Ndc1 interaction network in yeast nuclear pore complex assembly and maintenance. *J. Cell Biol.* 185:475–491. http://dx.doi.org/10.1083/jcb.200810030

Palladino, F., T. Laroche, E. Gilson, A. Axelrod, L. Pillus, and S.M. Gasser. 1993. SIR3 and SIR4 proteins are required for the positioning and integrity of yeast telomeres. *Cell.* 75:543–555. http://dx.doi.org/10.1016/0092-8674(93)90388-7

Pasupala, N., S. Easwaran, A. Hannan, D. Shore, and K. Mishra. 2012. The SUMO E3 ligase Siz2 exerts a locus-dependent effect on gene silencing in *Saccharomyces cerevisiae*. *Eukaryot. Cell.* 11:452–462. http://dx.doi.org/10.1128/EC.05243-11

Ptak, C., and R.W. Wozniak. 2016. Nucleoporins and chromatin metabolism. *Curr. Opin. Cell Biol.* 40:153–160. http://dx.doi.org/10.1016/j.ceb.2016.03.024

Ptak, C., J.D. Aitchison, and R.W. Wozniak. 2014. The multifunctional nuclear pore complex: A platform for controlling gene expression. *Curr. Opin. Cell Biol.* 28:46–53. http://dx.doi.org/10.1016/j.ceb.2014.02.001

Ramírez, F., D.P. Ryan, B. Grüning, V. Bhardwaj, F. Kilpert, A.S. Richter, S. Heyne, F. Dündar, and T. Manke. 2016. deepTools2: A next generation web server for deep-sequencing data analysis. *Nucleic Acids Res.* 44(W1):W160–W165. http://dx.doi.org/10.1093/nar/gkw257

Rosa, A., J.H. Maddocks, F.R. Neumann, S.M. Gasser, and A. Stasiak. 2006. Measuring limits of telomere movement on nuclear envelope. *Biophys. J.* 90:L24–L26. http://dx.doi.org/10.1529/biophysj.105.077974

Rout, M.P., J.D. Aitchison, A. Suprapto, K. Hjertaas, Y. Zhao, and B.T. Chait. 2000. The yeast nuclear pore complex: Composition, architecture, and transport mechanism. *J. Cell Biol.* 148:635–651. http://dx.doi.org/10.1083/jcb.148.4.635

Schober, H., H. Ferreira, V. Kalck, L.R. Gehlen, and S.M. Gasser. 2009. Yeast telomerase and the SUN domain protein Mps3 anchor telomeres and repress subtelomeric recombination. *Genes Dev.* 23:928–938. http://dx.doi.org/10.1101/gad.1787509

Stancheva, I., and E.C. Schirmer. 2014. Nuclear envelope: Connecting structural genome organization to regulation of gene expression. *Adv. Exp. Med. Biol.* 773:209–244. http://dx.doi.org/10.1007/978-1-4899-8032-8_10

Taddei, A., and S.M. Gasser. 2004. Multiple pathways for telomere tethering: functional implications of subnuclear position for heterochromatin formation. *Biochim. Biophys. Acta.* 1677:120–128. http://dx.doi.org/10.1016/j.bbaexp.2003.11.014

Taddei, A., and S.M. Gasser. 2012. Structure and function in the budding yeast nucleus. *Genetics.* 192:107–129. http://dx.doi.org/10.1534/genetics.112.140608

Taddei, A., F. Hediger, F.R. Neumann, C. Bauer, and S.M. Gasser. 2004. Separation of silencing from perinuclear anchoring functions in yeast Ku80, Sir4 and Esc1 proteins. *EMBO J.* 23:1301–1312. http://dx.doi.org/10.1038/sj.emboj.7600144

Taddei, A., H. Schober, and S.M. Gasser. 2010. The budding yeast nucleus. *Cold Spring Harb. Perspect. Biol.* 2:a000612. http://dx.doi.org/10.1101/cshperspect.a000612

Therizols, P., C. Fairhead, G.G. Cabal, A. Genovesio, J.C. Olivo-Marin, B. Dujon, and E. Fabre. 2006. Telomere tethering at the nuclear periphery is essential for efficient DNA double strand break repair in subtelomeric region. *J. Cell Biol.* 172:189–199. http://dx.doi.org/10.1083/jcb.200505159

Van de Vosse, D.W., Y. Wan, D.L. Lapetina, W.M. Chen, J.H. Chiang, J.D. Aitchison, and R.W. Wozniak. 2013. A role for the nucleoporin Nup170p in chromatin structure and gene silencing. *Cell.* 152:969–983. http://dx.doi.org/10.1016/j.cell.2013.01.049

Winey, M., D. Yarar, T.H. Giddings Jr., and D.N. Mastronarde. 1997. Nuclear pore complex number and distribution throughout the *Saccharomyces cerevisiae* cell cycle by three-dimensional reconstruction from electron micrographs of nuclear envelopes. *Mol. Biol. Cell.* 8:2119–2132. http://dx.doi.org/10.1091/mbc.8.11.2119

Wohlschlegel, J.A., E.S. Johnson, S.I. Reed, and J.R. Yates III. 2004. Global analysis of protein sumoylation in *Saccharomyces cerevisiae*. *J. Biol. Chem.* 279:45662–45668. http://dx.doi.org/10.1074/jbc.M409203200

Wu, A.C., and S.A. Rifkin. 2015. Aro: a machine learning approach to identifying single molecules and estimating classification error in fluorescence microscopy images. *BMC Bioinformatics.* 16:102. http://dx.doi.org/10.1186/s12859-015-0534-z